PPPL-5283

Ion gyroradius effects on particle trapping in kinetic Aflven waves along auroral field lines

P.A. Damiano, J.R. Johnson

August 2016

PRINCETON
PLASMA PHYSICS
LABORATORY

Princeton Plasma Physics Laboratory
Report Disclaimers

Full Legal Disclaimer

This report was prepared as an account of work sponsored by an agency of the United States Government. Neither the United States Government nor any agency thereof, nor any of their employees, nor any of their contractors, subcontractors or their employees, makes any warranty, express or implied, or assumes any legal liability or responsibility for the accuracy, completeness, or any third party's use or the results of such use of any information, apparatus, product, or process disclosed, or represents that its use would not infringe privately owned rights. Reference herein to any specific commercial product, process, or service by trade name, trademark, manufacturer, or otherwise, does not necessarily constitute or imply its endorsement, recommendation, or favoring by the United States Government or any agency thereof or its contractors or subcontractors. The views and opinions of authors expressed herein do not necessarily state or reflect those of the United States Government or any agency thereof.

Trademark Disclaimer

Reference herein to any specific commercial product, process, or service by trade name, trademark, manufacturer, or otherwise, does not necessarily constitute or imply its endorsement, recommendation, or favoring by the United States Government or any agency thereof or its contractors or subcontractors.

PPPL Report Availability

Princeton Plasma Physics Laboratory:

http://www.pppl.gov/techreports.cfm

Office of Scientific and Technical Information (OSTI):

http://www.osti.gov/scitech/

Related Links:

U.S. Department of Energy

U.S. Department of Energy Office of Science

U.S. Department of Energy Office of Fusion Energy Sciences

Ion gyroradius effects on particle trapping in kinetic Alfvén waves along auroral field lines

P.A. Damiano[1], J.R. Johnson[1], and C.C. Chaston[2,3]

- We investigate electron energization associated with trapping in kinetic Alfven waves.

- Ion gyroradius effects limit ability of kinetic Alfven wave to trap and energize electrons.

- Energized electron spectra at ionosphere are a sensitive function of ion temperature.

[1]Princeton Center for Heliophysics,

Princeton Plasma Physics Laboratory,

Princeton University, Princeton, NJ 08543

[2]Space Sciences Laboratory, University of

California, Berkeley, CA 94720

[3]School of Physics, University of Sydney,

Sydney, NSW 2006, Australia

Abstract.   In this study, a 2D self-consistent hybrid gyrofluid-kinetic electron model is used to investigate Alfvén wave propagation along dipolar magnetic field lines for a range of ion to electron temperature ratios. The focus of the investigation is on understanding the role of these effects on electron trapping in kinetic Alfvén waves sourced in the plasma sheet and the role of this trapping in contributing to the overall electron energization at the ionosphere. This work also builds on our previous effort [*Damiano et al.*, 2015] by considering a similar system in the limit of fixed initial parallel current, rather than fixed initial perpendicular electric field. It is found that the effects of particle trapping are strongest in the cold ion limit and the kinetic Alfvén wave is able to carry trapped electrons a large distance along the field line yielding a relatively large net energization of the trapped electron population as the phase speed of the wave is increased. However, as the ion temperature is increased, the ability of the kinetic Alfvén wave to carry and energize trapped electrons is reduced by more significant wave energy dispersion perpendicular to the ambient magnetic field which reduces the amplitude of the wave. This reduction of wave amplitude in-turn reduces both the parallel current and the extent of the high energy tails evident in the energized electron populations at the ionospheric boundary (which may serve to explain the limited extent of the broadband electron energization seen in observations). Even in the cold ion limit, trapping effects in kinetic Alfvén waves lead to only modest electron energization for the parameters considered (on

the order of tens of eV) and the primary energization of electrons to keV levels coincides with the arrival of the wave at the ionospheric boundary.

1. Introduction

Nonlinear trapping of electrons, leading to elongated beam like structures in the direction of parallel velocity are a ubiquitous feature of space plasmas. For example, such features have been noted in reconnection potentials [e.g. *Le et al.*, 2009], have been generated in active injection experiments in the ionosphere [e.g. *Haeusler et al.*, 1986; *Bohm et al.*, 1992], and are associated with kinetic Alfvén waves in the Earth's magnetosphere where they have been illustrated in Polar observations [e.g. *Wygant et al.*, 2002; *Janhunen et al.*, 2004] and have been reproduced in simulations [e.g. *Watt and Rankin*, 2009; *Damiano et al.*, 2015]. Such distributions are also observed in THEMIS observations of kinetic Alfvén waves in the plasma sheet (associated with the breaking of reconnection induced fast flows [e.g. *Chaston et al.*, 2012]) as illustrated in Figure 1 and more recently in Van Allen Probes observations associated with kinetic Alfvén wave activity in the inner magnetosphere [*Chaston et al.*, 2015].

In the auroral context, a fundamental question is how electron acceleration in these waves, which usually exist above the auroral acceleration region, might contribute to the energized precipitating electron population that ultimately leads to the generation of the visible aurora. As opposed to electron acceleration by inertial Alfvén waves in the auroral acceleration region (where $v_{th} \ll V_A$) kinetic Alfvén waves interact with electrons that have parallel velocities close to the phase speed of the wave. In a uniform topology, this leads to a modest parallel acceleration bounded by the trapping velocity associated with the wave potential ($v_{tr} = \sqrt{2e\phi/m_e}$ - e.g. *Bohm et al.* [1990, 1992]; *Wygant et al.* [2002]; *Rankin et al.* [2007]; *Le et al.* [2009]). However, in a non-uniform topology *Watt and*

Rankin [2009] noted that because the phase speed of kinetic Alfvén waves increases (due to the increasing magnetic field) as they propagate toward the ionosphere, the nonlinearly trapped electrons would be energized. Close to the intermediate regime along the field line (where $v_{th} \sim V_A$), the parallel electric field (and hence the trapping potential) would be progressively reduced and thus the energized, formerly trapped electrons, become free of the wave (which enters the inertial Alfvén wave regime due to the increasing Alfvén speed) and thus can propagate unimpeded to the ionosphere where they contribute to the precipitation of energized electrons.

One limitation of this analysis is that it was performed in the limit of cold ions, although in the plasma sheet, ion gyro radius effects are expected to be important because $T_i/T_e \sim 7$ [*Baumjohann et al.*, 1989]. *Damiano et al.* [2015] recently confirmed this point, by noting that the inclusion of ion temperature effects reduces the wave potential and consequently the effects of electron trapping. In the present paper we seek to build on this recent work by examining electron trapping in kinetic Alfvén waves sourced in the plasma sheet for a range of particle temperatures and wave amplitudes. Whereas in the previous effort, we considered how ion kinetic effects modify wave propagation given the same electric field driver amplitude, in this study we vary the amplitude of the initial perpendicular electric field to keep the initial parallel current characteristics constant and examine the evolution of the system in that context. The remainder of the paper is divided into three sections. Section 2 presents an overview of the hybrid gyrofluid-kinetic electron model that will be used in the investigation. Section 3 presents the simulation results while Section 4 draws conclusions based on this analysis.

2. Gyrofluid-Kinetic-Electron Model

The simulations are conducted with the hybrid 2-D Gyrofluid-Kinetic Electron (GKE) model discussed in [*Damiano et al.*, 2015] which is the gyrofluid extension of the hybrid MHD-kinetic electron model [*Damiano et al.*, 2003; *Damiano et al.*, 2007] that has seen extensive use in the study of field line resonances [e.g. *Damiano and Wright*, 2008; *Damiano and Johnson*, 2012]. The dipolar model geometry is illustrated in Figure 2a and explicitly includes the field aligned direction (x_1) and the direction across L shells (x_2). The system is independent of the azimuthal coordinate so that $\partial/\partial x_3 = 0$.

The gyrofluid portion of the model incorporates the modified linearized momentum equation given by

$$\mu_o \rho_o \frac{\partial \tilde{u}_3}{\partial t} = \frac{B_o}{h_1 h_3} \left(\frac{\partial}{\partial x_1} (h_3 b_3) \right) \tag{1}$$

where $\tilde{u}_3 = (1 - 1.25\rho_i^2 \nabla_\perp^2)u_3$ (and the coefficient of $\rho_i^2 \nabla_\perp^2$ is obtained from a Padé approximation [*Johnson and Cheng*, 1997; *Cheng and Johnson*, 1999]), ρ_i is the ion gyroradius, $x_1 = \cos\theta/r^2$, $x_2 = \sin^2\theta/r$, $x_3 = \phi$, $h_1 = r^3/(1 + 3\cos^2\theta)^{1/2}$, $h_2 = r^2/(\sin\theta(1 + 3\cos^2\theta)^{1/2})$, $h_3 = r\sin\theta$ and ρ_o and B_o denote the background plasma density and magnetic field respectively. This equation is coupled to Faraday's law

$$\frac{\partial b_3}{\partial t} = \frac{-1}{h_1 h_2} \left(\frac{\partial}{\partial x_1} (h_2 E_2) - \frac{\partial}{\partial x_2} (h_1 E_1) \right) \tag{2}$$

and the perpendicular

$$E_2 = -B_o(1 - \rho_i^2 \nabla_\perp^2)\tilde{u}_3 \tag{3}$$

and parallel Ohm's laws

$$E_{\|} = \frac{m_e}{ne^2}\frac{\partial j_{\|}}{\partial t} - \frac{1}{ne}\nabla_{\|}P_{e_{\|}} - \frac{1}{ne}\frac{P_{e_{\|}} - P_{e_\perp}}{B_o}\nabla_{\|}B_o \tag{4}$$

where the first term on the right hand side yields the electron inertial contribution, the second term yields the electron pressure contribution (kinetic Alfvén wave) and the last term incorporates the mirror force effects. It should be noted that the parallel generalized Ohm's law is not solved in the model in this form. We have displayed the law here in conventional form and without metric tensor coefficients for simplicity of notation and understanding. The full form of the parallel Ohm's law is apparent in several other previous publications (including *Damiano et al.* [2015]) and the full derivation can be found in *Damiano et al.* [2007].

The guiding center equations are used to describe the parallel electron dynamics

$$m_e\frac{dv_1}{dt} = -eE_1 - \mu_m\frac{1}{h_1}\frac{\partial B_o}{\partial x_1} \tag{5}$$

$$h_1\frac{dx_1}{dt} = v_1 \tag{6}$$

where $v_1 = v_{\|}$ is the parallel electron velocity and $\mu_m =$ is the magnetic moment. Conservation of μ_m is assumed in the model and the value of $v_\perp$ computed at any given time from μ_m is the gyrophase independent perpendicular velocity ($v_\perp = \sqrt{v_2^2 + v_3^2}$). Standard Particle-In-Cell techniques (as discussed in *Damiano et al.* [2007]) are used to compute the integral moments of the electron distribution function for use in the parallel Ohm's law.

3. Simulations

Consistent with *Damiano et al.* [2015], the simulation grid extends from the $L = 9.4$ to the $L = 10$ field lines in the perpendicular direction and the low altitude boundaries are set to a geocentric altitude of 2 R_E. This altitude was chosen as it corresponds to the average location of the B/n peak (where the peak of the electron acceleration is believed to occur [*Swift*, 1978; *Lysak and Hudson*, 1979; *Wright et al.*, 2002; *Damiano and Wright*, 2008]). Electrons are initially positioned to form a constant density such that $n_i = n_e = 1$ cm^{-3} (which is order of magnitude consistent with densities measured at altitudes above 2 R_E [e.g. *Kletzing and Torbert*, 1994]) and equal temperature Maxwellians are assumed in both $v_\perp$ and $v_\parallel$.

The dispersive Alfvén waves are initiated in the equatorial plane of the simulation domain by perturbing the azimuthal velocity at $t = 0$ (which is equivalent to perturbing the ion polarization current). The perpendicular profile of the perturbations assumed is equivalent to those used in *Damiano et al.* [2015] and is displayed in Figure 2b. For a $T_i = 1$ keV ion temperature, this profile leads to a value of $k_\perp \rho_i \sim 1$ in the plasma sheet (where the field aligned profiles of ρ_i and V_A are plotted in Figure 3). In this present study, although we do not adjust the perpendicular profile of the perturbation, a range of amplitudes and ion temperatures are considered. In the parallel direction, a Gaussian with a full width half maximum of 1 R_E is chosen. This profile splits up into two equivalent perturbations traveling to the northern and southern low altitude boundaries respectively. As in *Damiano et al.* [2015], our analysis will focus on wave perturbations propagating to the northern low altitude boundary, as the evolution of the system is symmetric in both directions.

3.1. Particle trapping in kinetic Alfvén waves

In this section, we consider the evolution of the system without ion Larmor radius effects ($T_i = 0$). Figure 4a illustrates the evolution of the parallel current as a function of time for the E_2 perturbation presented in Figure 2b and $T_e = 100$ eV (this value of T_e will be fixed for the whole investigation). The electron distribution functions at $l_\parallel = 2 \ R_E$ (where $l_\parallel$ is measured from the equator) for the indicated times are presented in Figures 4b-4d. As the wave perturbations reach $l_\parallel = 2 \ R_E$, the initial Maxwellian distribution function transitions to one with a pronounced parallel elongation consistent with *Damiano et al.* [2015]. However, the initial perpendicular electric field of this simulation is larger than that used in *Damiano et al.* [2015] and the distributions are plotted closer to the equatorial plane in order to see more clearly the effects of trapping.

As mentioned in *Damiano et al.* [2015], the parallel extent of the elongation is defined by the trapping width, $v_{tr} = \sqrt{2e\phi/m_e}$. To confirm this point, we have calculated the potential $\phi = -\int E_\parallel d_\parallel$ for the pulse perturbation at $t = 15$ s in Figure 4c. The result is illustrated in Figure 5 where the position of the peak of the potential is consistent with the peak of the parallel current illustrated in Figure 4. Taking the value of the peak potential (~ 62 eV), the value of the trapping width is found to be 0.48×10^7 m/s. To make this comparison clearer, in Figure 6 we re-plot the distribution functions from Figure 4 as a function of $v_\parallel$ alone where the dashed vertical lines are indicative of $\pm v_{tr}$ based on the peak potential determined from Figure 5. As expected, the plateau region agrees quite well with the boundaries defined by $\pm v_{tr}$.

The trapped nature of these electrons is further elucidated in Figure 7 where we plot the time history of the electrons within the trapped region as illustrated in Figure 6c (although

we have only taken a narrow subset of the trapped population defined by $|v_{||}| < 1.5 \times 10^6$

m/s). Superimposed in this figure is the distance vs time relationship (solid red line)

assuming the initial phase speed of the wave (as determined from the dispersion relation

$\omega = k_{||}V_A$ which does not change much over the first 2 R_E) and it is clear that the

electrons travel as a coherent group trapped within the potential well of the wave. When

the same analysis is applied to a group of untrapped electrons, there is no consistent

evolution with the wave in the time history (not shown). Figure 7b plots the average

electron kinetic energy of the same trapped electrons as a function of time and there is

both an oscillation in the average energy (associated with the exchange between kinetic

and potential energy) and a slow increase in the average energy with time as the phase

speed of the wave increases (consistent with the idea of *Watt and Rankin* [2009]). The

average energy increases by a few tens of eV before plateauing when the electrons become

detrapped from the wave at about $t = 30$ seconds.

Also from Figure 7a, it is clear that the trapping goes back to the wave initialization

at $t = 0$. As mentioned previously, there is no current at $t = 0$. The initial perturbation

in $E_\perp$, which peaks at the equator, breaks up into two perturbations which travel to the

opposing low altitude boundaries. The growth of the current perturbation in the northern

hemisphere of the simulation domain over the first few seconds is plotted in Figure 8a

along with the distribution functions at $l_{||} = 0.5$ R_E. This growth is significantly faster

than the parallel propagation and so it is informative to look at the temporal evolution

of the distribution function at one point in space (Figures 8b - 8d). Initially, electrons

with $v_{||} \sim v_{ph} \sim V_A$ (close to the core of the electron distribution), are trapped by the

waves but this trapping extends to larger values of $|v_\parallel|$ as the parallel current density (and consequently trapping potential) in the wave grows.

3.2. Gyroradius effects on wave trapping

As discussed in *Damiano et al.* [2015], the inclusion of ion gyroradius effects reduces the noted parallel elongation (relative to the $T_i = 0$ case) (for a given value of the perpendicular electric field) since the inclusion of these effects reduces the ability of the wave to carry a parallel current (because the perturbation is not able to drive a strong polarization current in the hot ion limit) thus reducing both $E_\parallel$ and ϕ. This point is re-iterated in Figures 9a and 9b where a reduced parallel current is evident in the blue case ($T_i = 1$ keV) relative to the black case ($T_i = 0$) even though the magnitude of the perpendicular electric field remains the same between the two cases (Figure 9b). The corresponding reduced elongation is reflected in a comparison of Figures 9d and 9c. As with *Damiano et al.* [2015], we have plotted the $T_i = 1$ keV case at an earlier time than the $T_i = 0$ case since the wave speed increases with the inclusion of ion gyroradius effects as given by the dispersion relation

$$\omega = k_\parallel V_A \sqrt{1 + k_\perp^2 \rho_i^2 (1 + \frac{T_e}{T_i}))}. \tag{7}$$

However, if we then increase the initial E_2 perturbation in the $T_i = 1$ keV case, so that we end up with a similar parallel current as in the $T_i = 0$ case (comparing red and black lines in Figures 9a and 9b), the parallel elongation in the $T_i = 0$ case approaches that evident in the $T_i = 0$ case, but is still slightly less (comparing Figures 9e and 9d). This result is consistent with having a similar parallel current because the current is carried by

a slight asymmetry of the distribution around $v_\parallel = 0$ and not the length of the elongated region.

It is then of particular interest to understand how perturbations carrying a similar current evolve in the two different ion temperature regimes. The time history of the trapped electrons illustrated in Figures 9c and 9e are plotted in Figures 10a and 10c (while a corresponding example for $T_i = 500$ eV is plotted in Figure 10b). Even though the parallel elongation of the distribution functions at $l_\parallel = 1.85$ R_E is similar in all cases, the time and length of the trapping decreases as T_i/T_e increases. The reduced trapping time as a function of the increasing temperature ratio is reflected in a reduced total energization when the average kinetic energy of the trapped electrons is plotted as a function of time (Figure 10d). Interestingly, the period of the cycling in E_K decreases with increases in T_i/T_e as well. Defining the trapping period $\tau = \int dl/v_\parallel$ and assuming a Gaussian shaped potential ϕ (e.g. as displayed in Figure 5), it is straightforward to show that $\tau \sim 1/\sqrt{\phi}$. Therefore, since ϕ is decreasing with the increase in ion temperature, the increase in the oscillation period with ion temperature evident in Figure 10c is consistent with this analysis.

In order to illuminate the reason for the reduced trapping, Figure 11 plots the profile of the parallel current (and the corresponding electron distribution functions at the current maxima) at several times for the $T_i = 0$ case (left hand panels) and the $T_i = 1$ keV case (right hand panels). The times were chosen so that the current profiles for the two different cases peak at the same positions in space. In the $T_i = 0$ case, the parallel current density of the wave increases in amplitude as the wave propagates toward the northern low altitude boundary, which is consistent with the converging magnetic field topology. Consistent with

the evolution in current, the parallel elongation in the distribution function decreases as $E_\parallel$ drops as the pulse gets closer to the transition region between the kinetic Alfvén wave and inertial Alfvén wave regimes.

In Figure 11e, the evolution of the parallel current in the $T_i = 1$ keV case is qualitatively different from the $T_i = 0$ case as the amplitude of the parallel current profile seems relatively constant (actually decreasing marginally) relative to the $T_i = 0$ case. Consistent with the drop in current, the parallel elongation in the electron distribution functions evident in the $T_i = 1$ keV case reduces relative to the $T_i = 0$ case. This trend is evident primarily in the comparison of the distribution functions at $l_\parallel = 2$ and $l_\parallel = 3.5$ R_E. By $l_\parallel = 5$ R_E, most significant trapping effects are minimized (refer to Figure 10) and the distribution functions in Figures 11d and 11h are reflective of largely untrapped populations. There is slightly more asymmetry in the positive $v_\parallel$ direction in Figure 11d relative to Figure 11h reflective of the higher parallel current in the $T_i = 0$ case. Additionally, mirror force effects contribute to a slight horseshoe shape in the core of the distributions as the pulse gets closer to the northern low altitude boundary.

This difference in the current evolution in the $T_i = 0$ and $T_i = 1$ keV cases can be understood from the profiles of E_2 plotted in Figure 9b. The $T_i = 1$ keV cases exhibit a broader perpendicular dispersion of wave energy relative to the $T_i = 0$ case since with $k_\perp \rho_i \sim 1$ a larger perpendicular group speed results (see equation 7) which moves energy away in both directions from the region of peak current in the middle of the simulation domain. There is also a moderately more pronounced dispersion of wave energy parallel to the field line in the $T_i = 1$ keV case, but the parallel dispersion is of secondary importance

relative to the perpendicular dispersion (which moves wave energy entirely off the field line of interest).

As Landau damping effects are known to contribute to wave energy dissipation in kinetic Alfvén waves, there might be some expectation that the drop in amplitude between the $T_i = 0$ and $T_i = 1$ keV cases might also be associated with energy dissipation due to wave-particle interactions with electrons. However, this cannot be the case as the inclusion of ion gyroradius effects, while keeping all other parameters the same, decreases the efficiency of the Landau damping because of the increased phase speed of the wave moves the resonance condition between the electrons and the wave more into the tail of the distribution function where fewer particles can interact with the wave. This effect is also evident from the dispersion relation analysis in *Lysak and Lotko* [1996].

3.3. Effects of T_e/T_i ratio on ionospheric electron energization

In *Damiano et al.* [2015], we plotted the distribution of electrons at the ionospheric boundary coincident with the arrival of the wave considering simulations with $T_i = 0$ and $T_i = 1$ keV, but with the same initial E_2. A reduced energy spectrum was found in the $T_i = 1$ keV case since the parallel current was reduced in the wave for a given value of E_2. In the present example, we have considered cases with $T_i = 0$ and $T_i = 1$ keV where E_2 has been chosen so that the parallel current profiles are initially similar. The temporal evolution of the ionospheric current, along with the ionospheric electron energy spectrum at the current maximum, is in each case displayed in Figure 12 along with the $T_i = 500$ eV case. From this figure, it is clear that although the initial current in all cases was initialized to be the same, the peak ionospheric current reduces as the ion to electron

temperature ratio increases (as does the extent of the high energy tail plotted in Figure 12b).

Indeed, observations indicate that the extent of the electron energization in broadband aurora is generally only on the order of several hundred eV to a keV [e.g. *Chaston et al.*, 2002; *Chaston*, 2006] and so these simulation results suggest that ion gyroradius effects (in a warmer plasma sheet) may be a factor in limiting this energization. Additionally, kinetic Alfvén waves can stochastically heat ions perpendicular to the ambient magnetic field [e.g. *Johnson and Cheng*, 2001] (as seen in THEMIS plasma sheet observations [*Chaston et al.*, 2014]). Therefore, the simulations results also suggest that a gradual shutting off of broadband auroral precipitation may occur as the ion temperature increases over time.

In the inertial Alfvén wave regime close to the ionospheric boundary, there is both a resonant (Fermi) and non-resonant contribution to the electron energization [e.g. *Kletzing*, 1994; *Watt et al.*, 2005, 2006]. This non-resonant component is associated with the bulk energization of the distribution to carry the parallel current in the inertial Alfvén wave and was noted by *Watt et al.* [2005, 2006] to account for the suprathermal electron bursts evident in FAST satellite data. In *Damiano et al.* [2015], we illustrated that the main electron energization at the ionospheric boundaries evident in Figure 12 was occurring at the same time as the arrival of the wave and thus associated with this non-resonant acceleration. We found no significant resonant Fermi accelerated component (which is mostly likely because of the wave and plasma parameters chosen). The same scenario is true in this manuscript. Although the particle trapping effect in the kinetic Alfvén waves plays a role in the energization of the electrons, it is of limited significance for the

parameters considered here as the energy gains are limited to tens of eV for the best case scenario in the limit of $T_i = 0$ (see Figure 10).

Finally, it is worth noting that it has not been our aim in this study to quantitatively address electron energization in dispersive scale Alfvén waves for a wide range of observed magnetospheric parameters. Our primary aim has been to understand ion gyroradius effects on electron trapping in kinetic Alfvén waves for the more controlled set of plasma conditions consistent with our previous effort [*Damiano et al.*, 2015] in order to facilitate comparison of the case of fixed initial current with that of fixed initial perpendicular electric field. However, we want to emphasize that our choice of wave parameters are representative of average parameters associated with Alfvén waves as seen by both THEMIS [e.g. *Chaston et al.*, 2012, 2014] and Polar [e.g. *Keiling et al.*, 2001]. Additionally, while our choice of individual plasma temperatures is on the colder side, they are relevant to the generation of broadband aurora that form under conditions of northward IMF [S. Wing, private communication regarding *Luhr et al.*, submitted 2016] that can often be associated with the formation of a Cold Dense Plasma Sheet (CDPS - e.g. *Wing et al.* [2005]; *Johnson and Wing* [2009]). A systematic investigation of the warmer plasma limit, with parameters directly derived from THEMIS observations, is in progress and will be the focus of a follow-up manuscript.

4. Conclusions

Building on the work of *Damiano et al.* [2015], we have used the 2D hybrid GKE model to study the electron response to dispersive scale Alfvén waves propagating along auroral field lines for a range of ion temperatures and wave amplitudes. Consistent with previous efforts, we find that electrons trapped in the source region of the wave can be carried

along the field line and energized by the wave. We find that the effects of this trapping are strongest in the cold ion limit, and the trapping diminishes in effectiveness as the ion temperature is increased.

This reduction is partially due to the reduction of the ability of the wave to carry a parallel current (as noted in *Damiano et al.* [2015]) which decreases the magnitude of the trapping parallel electric field. Increasing the amplitude of the wave increases the effectiveness of the trapping, but in the hot ion limit, dispersion of wave energy perpendicular to the ambient magnetic field reduces the wave amplitude along a given field line limiting again both the parallel current and trapping potential ϕ meaning that particles become untrapped sooner than in the $T_i = 0$ limit. The reduced parallel current also results in reduced electron energization at the ionospheric boundary as manifested in shorter high energy tails in the electron spectra evident there. Therefore, the ion temperature appears to be an important factor in defining the characteristics of the precipitating electron spectra principally because of its effects on the dispersive characteristics of the wave.

Finally, for the parameters we have considered here, particle trapping in kinetic Alfvén waves sourced in the plasma sheet leads to only modest electron energization (tens of eV in the cold ion limit) and the primary energization of electrons to high energies is happening above the ionospheric boundary coincident with the arrival of the wave.

References

Baumjohann, W., G. Paschmann, and C. A. Cattell (1989), Average plasma properties in the central plasma sheet, *J. Geophys. Res., , 94*, 6597–6606, doi:10.1029/JA094iA06p06597.

Bohm, M., N. Brenning, and C.-G. Fälthammar (1990), Dynamic trapping: Neutralization of positive space charge in a collisionless magnetized plasma, *Physical Review Letters, 65*, 859–862, doi:10.1103/PhysRevLett.65.859.

Bohm, M., N. Brenning, and C.-G. Faelthammar (1992), Dynamic trapping of electrons in the porcupine ionospheric ion beam experiment, *Advances in Space Research, 12*, 9–14, doi:10.1016/0273-1177(92)90344-W.

Chaston, C. C. (2006), ULF Waves and Auroral Electrons, in *Magnetospheric ULF Waves: Synthesis and New Directions, Washington DC American Geophysical Union Geophysical Monograph Series*, vol. 169, edited by K. Takahashi, P. J. Chi, R. E. Denton, and R. L. Lysak, p. 239.

Chaston, C. C., J. W. Bonnell, C. W. Carlson, M. Berthomier, L. M. Peticolas, I. Roth, J. P. McFadden, R. E. Ergun, and R. J. Strangeway (2002), Electron acceleration in

the ionospheric Alfven resonator, *Journal of Geophysical Research (Space Physics)*, *107*, 1413, doi:10.1029/2002JA009272.

Chaston, C. C., J. W. Bonnell, L. Clausen, and V. Angelopoulos (2012), Energy transport by kinetic-scale electromagnetic waves in fast plasma sheet flows, *Journal of Geophysical Research (Space Physics)*, *117*, A09202, doi:10.1029/2012JA017863.

Chaston, C. C., J. W. Bonnell, and C. Salem (2014), Heating of the plasma sheet by broadband electromagnetic waves, *Geophys. Res. Lett.,* , *41*, 8185–8192, doi: 10.1002/2014GL062116.

Chaston, C. C., J. W. Bonnell, J. R. Wygant, C. A. Kletzing, G. D. Reeves, A. Gerrard, L. Lanzerotti, and C. W. Smith (2015), Extreme ionospheric ion energization and electron heating in Alfvén waves in the storm time inner magnetosphere, *Geophys. Res. Lett.,* , *42*, 10, doi:10.1002/2015GL066674.

Cheng, C. Z., and J. R. Johnson (1999), A kinetic-fluid model, *J. Geophys. Res.,* , *104*, 413–428, doi:10.1029/1998JA900065.

Damiano, P. A., and J. R. Johnson (2012), Electron acceleration in a geomagnetic Field Line Resonance, *Geophys. Res. Lett.,* , *39*, L02102, doi:10.1029/2011GL050264.

Damiano, P. A., and A. N. Wright (2008), Electron thermal effects in standing shear Alfvén waves, *Journal of Geophysical Research (Space Physics)*, *113*, A09219, doi: 10.1029/2008JA013087.

Damiano, P. A., R. D. Sydora, and J. C. Samson (2003), Hybrid magnetohydrodynamic-kinetic model of standing shear Alfvén waves, *Journal of Plasma Physics*, *69*, 277–304, doi:10.1017/S0022377803002216.

Damiano, P. A., A. N. Wright, R. D. Sydora, and J. C. Samson (2007), Energy dissipation via electron energization in standing shear Alfvén waves, *Phys. Plasmas*, *14*, 062,904.

Damiano, P. A., J. R. Johnson, and C. C. Chaston (2015), Ion temperature effects on magnetotail Alfvén wave propagation and electron energization, *Journal of Geophysical Research (Space Physics)*, *120*, 5623–5632, doi:10.1002/2015JA021074.

Haeusler, B., R. A. Treumann, O. H. Bauer, G. Haerendel, and R. Bush (1986), Observations of the artificially injected Porcupine xenon ion beam in the ionosphere, *J. Geophys. Res.*, , *91*, 287–303, doi:10.1029/JA091iA01p00287.

Janhunen, P., A. Olsson, J. Hanasz, C. Russell, H. Laakso, and J. Samson (2004), Different Alfvén wave acceleration processes of electrons in substorms at ~4-5 RE and 2-3 RE radial distance, *Annales Geophysicae*, *22*, 2213–2227, doi:10.5194/angeo-22-2213-2004.

Johnson, J. R., and C. Z. Cheng (1997), Kinetic Alfvén waves and plasma transport at the magnetopause, *Geophys. Res. Lett.*, *24*, 1423–1426, doi:10.1029/97GL01333.

Johnson, J. R., and C. Z. Cheng (2001), Stochastic ion heating at the magnetopause due to kinetic Alfvén waves, *Geophys. Res. Lett.*, , *28*, 4421–4424, doi:10.1029/2001GL013509.

Johnson, J. R., and S. Wing (2009), Northward interplanetary magnetic field plasma sheet entropies, *Journal of Geophysical Research (Space Physics)*, *114*, A00D08, doi: 10.1029/2008JA014017.

Keiling, A., J. R. Wygant, C. Cattell, M. Johnson, M. Temerin, F. S. Mozer, C. A. Kletzing, J. Scudder, and C. T. Russell (2001), Properties of large electric fields in the plasma sheet at formula alphabet="latin"4-7R_E measured with Polar, *J. Geophys. Res.*, , *106*, 5779–5798, doi:10.1029/2000JA900130.

Kletzing, C. A. (1994), Electron acceleration by kinetic Alfvén waves, *J. Geophys. Res.,*
, *99*, 11,095–11,104, doi:10.1029/94JA00345.

Kletzing, C. A., and R. B. Torbert (1994), Electron time dispersion, *J. Geophys. Res.,* ,
99, 2159–2172, doi:10.1029/93JA01745.

Le, A., J. Egedal, W. Daughton, W. Fox, and N. Katz (2009), Equations of State for
Collisionless Guide-Field Reconnection, *Physical Review Letters*, *102*(8), 085001, doi:
10.1103/PhysRevLett.102.085001.

Luhr, H., T. Huang, S. Wing, G. Kervalishvili, J. Rauberg, and K. H. (submitted 2016),
Special features of field-aligned currents at high latitudes during northward pointing in-
terplanetary magnetic field derived with the swarm constellation, *Annales Geophysicae.*

Lysak, R. L., and M. K. Hudson (1979), Coherent anomalous resistivity in the region of
electrostatic shocks, *Geophys. Res. Lett.*, *6*, 661–663, doi:10.1029/GL006i008p00661.

Lysak, R. L., and W. Lotko (1996), On the kinetic dispersion relation for shear Alfvén
waves, *J. Geophys. Res.,* , *101*, 5085–5094, doi:10.1029/95JA03712.

Rankin, R., C. E. J. Watt, and J. C. Samson (2007), Self-consistent wave-particle inter-
actions in dispersive scale long-period field-line-resonances, *Geophys. Res. Lett.,* , *34*,
L23103, doi:10.1029/2007GL031317.

Swift, D. W. (1978), Mechanisms for the discrete aurora - A review, *Space Science Review*,
22, 35–75, doi:10.1007/BF00215813.

Watt, C. E. J., and R. Rankin (2009), Electron Trapping in Shear Alfvén
Waves that Power the Aurora, *Physical Review Letters*, *102*(4), 045002, doi:
10.1103/PhysRevLett.102.045002.

Watt, C. E. J., R. Rankin, I. J. Rae, and D. M. Wright (2005), Self-consistent electron acceleration due to inertial Alfvén wave pulses, *Journal of Geophysical Research (Space Physics)*, *110*, A10S07, doi:10.1029/2004JA010877.

Watt, C. E. J., R. Rankin, I. J. Rae, and D. M. Wright (2006), Inertial Alfvén waves and acceleration of electrons in nonuniform magnetic fields, *Geophys. Res. Lett., , 33*, L02106, doi:10.1029/2005GL024779.

Wing, S., J. R. Johnson, P. T. Newell, and C.-I. Meng (2005), Dawn-dusk asymmetries, ion spectra, and sources in the northward interplanetary magnetic field plasma sheet, *Journal of Geophysical Research (Space Physics)*, *110*, A08205, doi:10.1029/2005JA011086.

Wright, A. N., W. Allan, M. S. Ruderman, and R. C. Elphic (2002), The dynamics of current carriers in standing Alfvén waves: Parallel electric fields in the auroral acceleration region, *J. Geophys. Res.*, *107*, 1120.

Wygant, J. R., et al. (2002), Evidence for kinetic Alfvén waves and parallel electron energization at 4-6 R_E altitudes in the plasma sheet boundary layer, *Journal of Geophysical Research (Space Physics)*, *107*, 1201-+, doi:10.1029/2001JA900113.
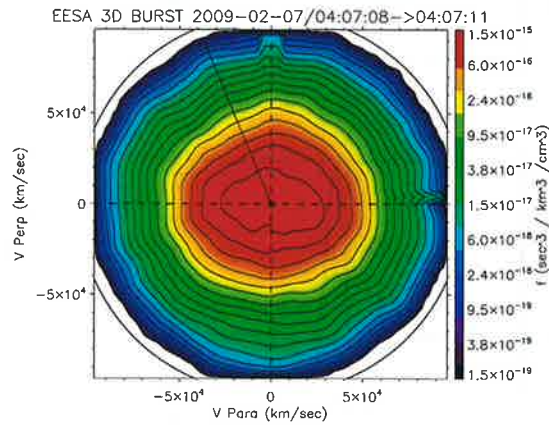
Figure 1.   Example of electron distribution observed in THEMIS D spacecraft data in plasma sheet associated with KAW activity. Note the elongated core in the parallel direction which is qualitatively similar to the distributions generated in the simulations presented in this study.
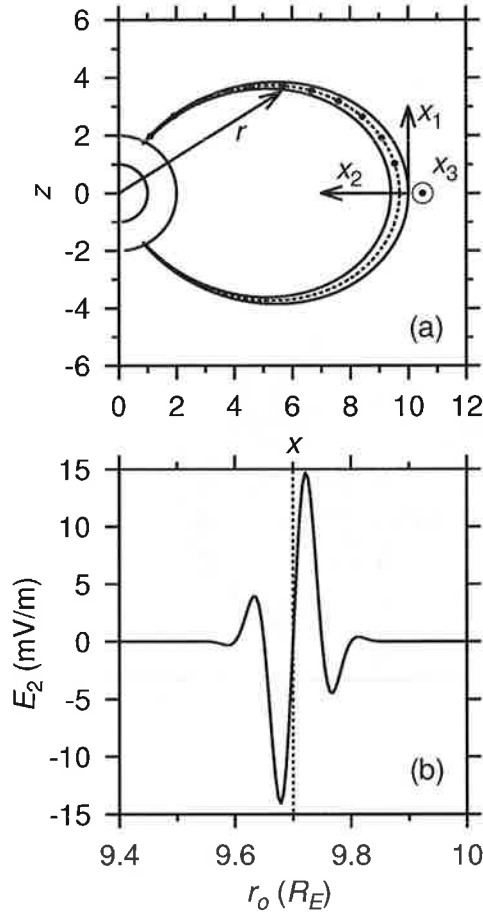
Figure 2. a): Simulation domain where x_3 is positive increasing out of the page. Solid lines denote the $L = 9.4$ and $L = 10$ perpendicular boundary field lines. The dotted line indicates the $L = 9.7$ field line (along which the maximum parallel current of the wave perturbation occurs) where the solid dots denote 1 R_E length intervals along the field line. The circles of radius 1 and 2 R_E respectively denote the surface of the Earth and low altitude "ionospheric" boundary. b) Initial radial (E_2) electric field profile (used in Section 3.1) as a function of r_o ($r = r_o \sin \theta$, where the angle θ is subtended from the z axis) at the equator for $L_\perp = 0.1 \ R_E$.
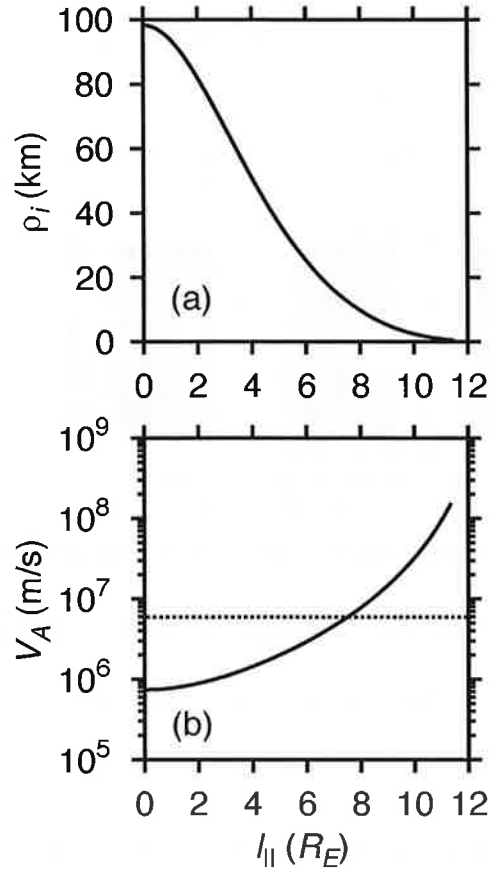
Figure 3.   a) Ion gyroradius profile for $T_i = 1$ keV as a function of length along the field line ($l_{||}$) measured from the equator in R_E. b) Alfvén velocity profile as a function of $l_{||}$. The dotted horizontal line denotes $v_{th} = V_A$. Both profiles are taken along $L = 9.7$ field line.
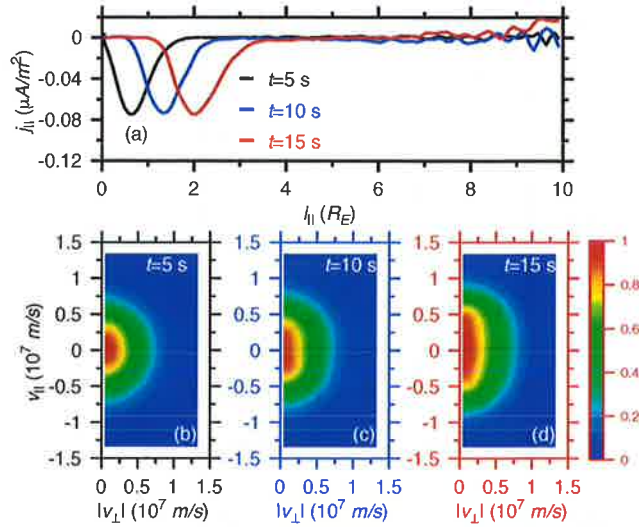
Figure 4.   a) Parallel current density along the $L = 9.7$ field line at indicated times.
(b) Electron velocity distribution function (normalized) at $l_\parallel = 2\ R_E$ for the black case
(panel a). (c) same as (b), but for blue case in panel (a). (d) Same again, but for red
case. Small scale fluctuations evident to the right in panel (a) result from statistical noise
near the low altitude boundary where the number of simulation particles per grid cell is
less than in the the equatorial region. However, the fluctuation levels are far smaller than
the signal when the wave reaches the lower altitude boundary as seen in Figure 12.
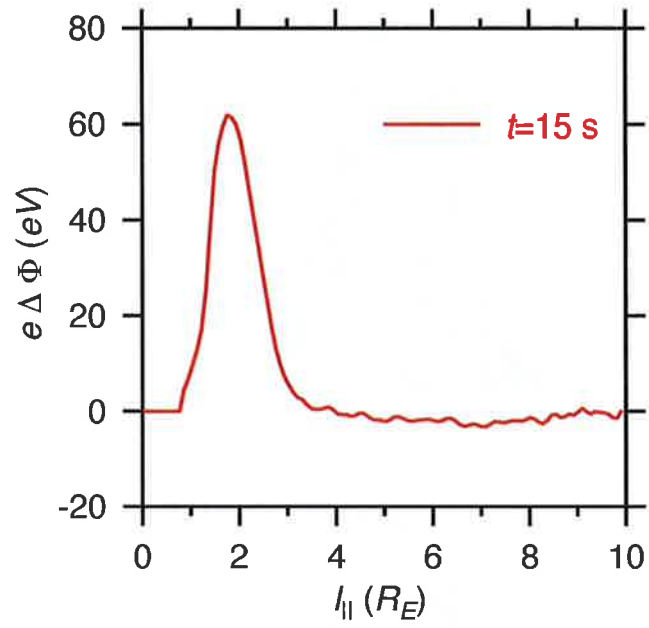
Figure 5.   (a) Potential, $\phi = -\int E_{\parallel} dl$, of the pulse associated with the red line in Figure 4.
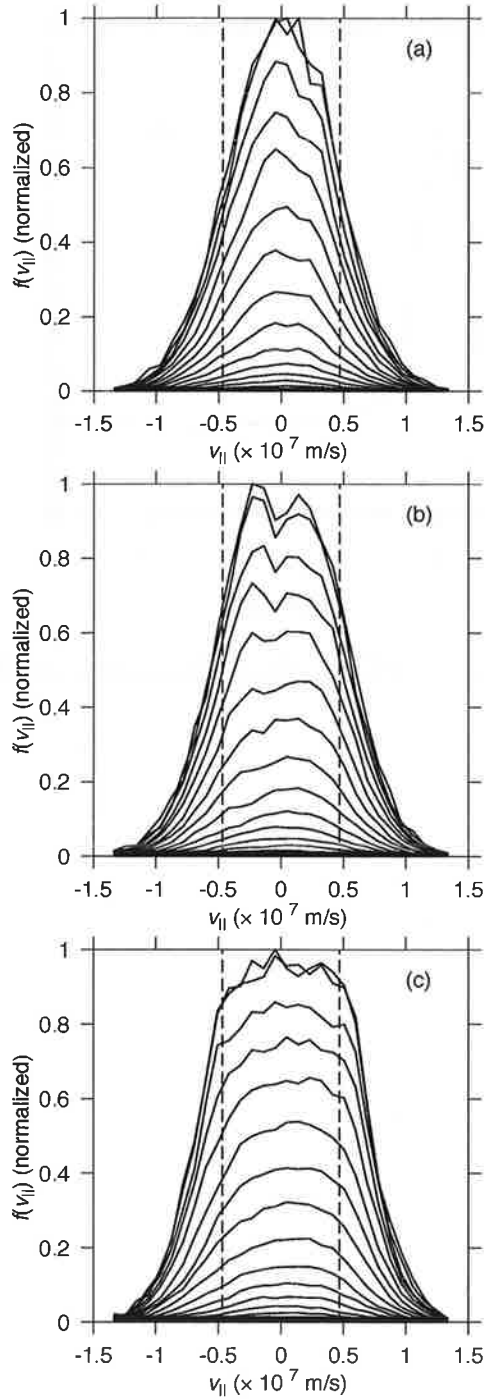
Figure 6.   a) Electron distribution function as a function of $v_{\parallel}$ at the same times used in Figure 4. Sold black lines are indicative of different values of $v_{\perp}$. The vertical dashed lines in each panel indicate $v_{tr} = \pm\sqrt{2e\phi/m_e}$ using the maximum of the potential, ϕ, as defined by the peak displayed in Figure 5.
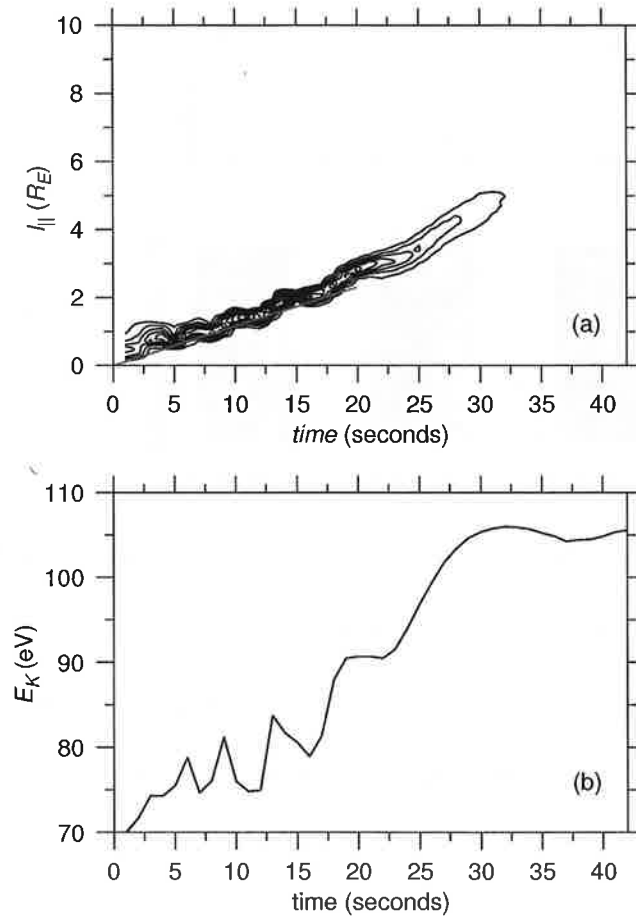
Figure 7. (a) Distribution of electrons along the $L = 9.7$ field line as a function of time

for electron population trapped in the kinetic Alfvén wave at t=15 seconds (and $l_{\parallel} = 2$

R_E). Example taken from the $T_i = 0$ case considered in Figures 4 and 6. Plots were

created by taking the positions of the relevant electrons, at each time and binning them

as a function of distance along the field line. The solid red line shows the trajectory based

on the original phase speed of wave (which does not vary significantly over the plotted

interval). (b) Average kinetic energy (E_K) of trapped electrons considered in panel (a) as

a function of time.
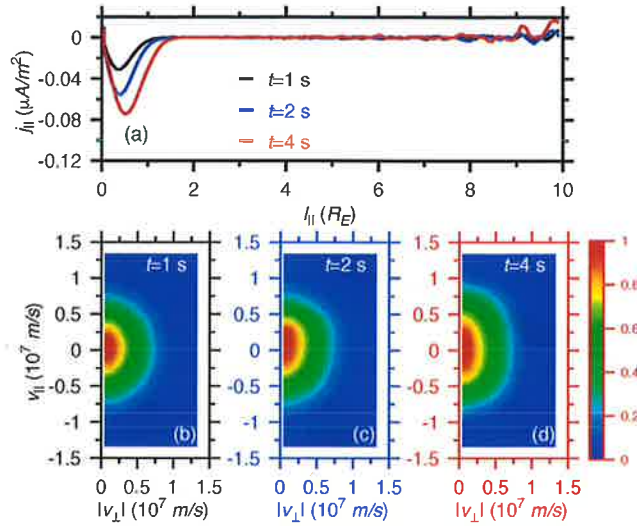
Figure 8.   a) Parallel current density along the $L = 9.7$ field line at indicated times. (b)-(d) electron velocity distribution function (normalized) at $l_{||} = 0.5\ R_E$ at indicated times. The trapping width increases as the current (and hence potential) in the wave grows. The initial temperature of the distribution function is 100 eV.
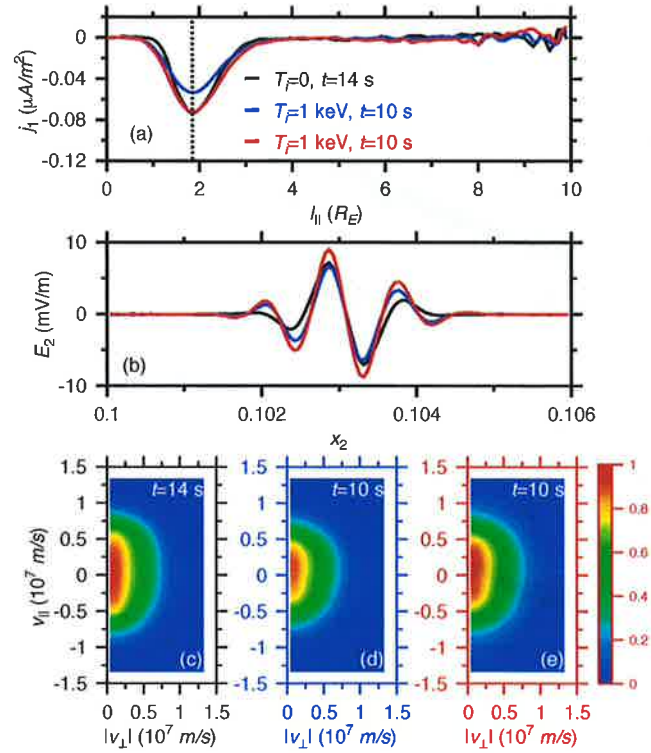
Figure 9. a) Parallel current density along the $L = 9.7$ field line for indicated times and ion temperatures. In all cases $T_e = 100$ eV. Times have been chosen so that maxima overlap at $l_{||} = 1.85\ R_E$ (dotted black line). b) Perpendicular profile of E_2 at $l_{||} = 1.85\ R_E$ in all three cases. d) Electron velocity distribution function (normalized) at same position for black case in panel (a). e) Same as d), but for blue case in panel (a). f) Same again, but for red case in panel (a).
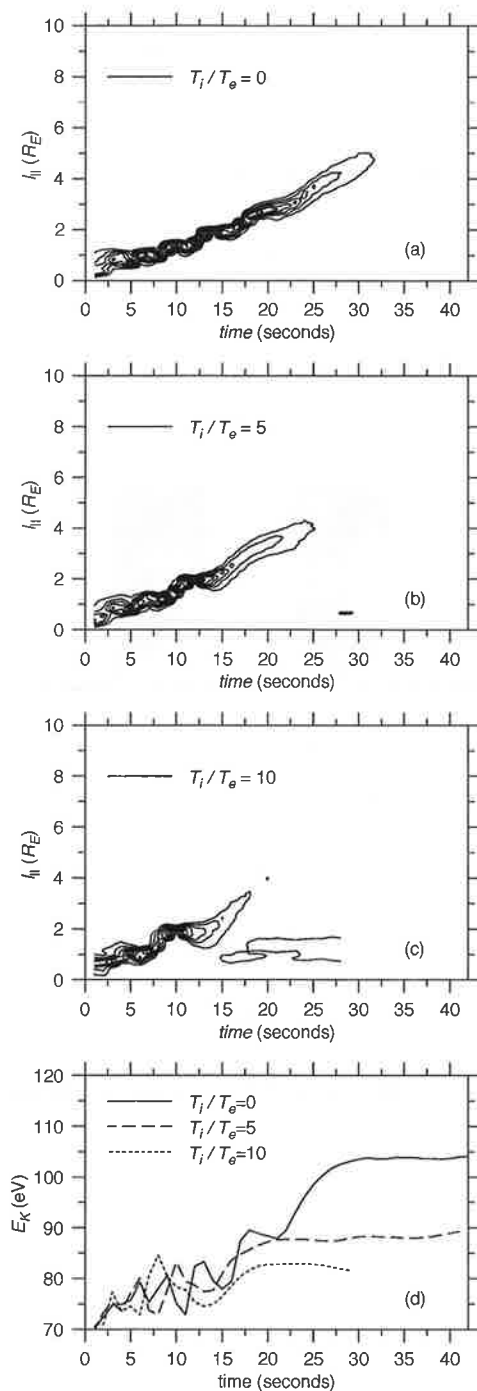
Figure 10. (a) Distribution of electrons along the $L = 9.7$ field line as a function of time for electron population trapped in the kinetic Alfvén wave at $l_{\parallel} = 1.85\ R_E$ for $T_i/T_e = 0$ case. (b) Same as (a), but for $T_i/T_e = 5$ case. (c) Same as (a), but for $T_i/T_e = 10$ case. (d) Average kinetic energy (E_K) of trapped electrons considered in panel (a) (solid line), panel (b) (dashed line) and panel (c) (dotted line).
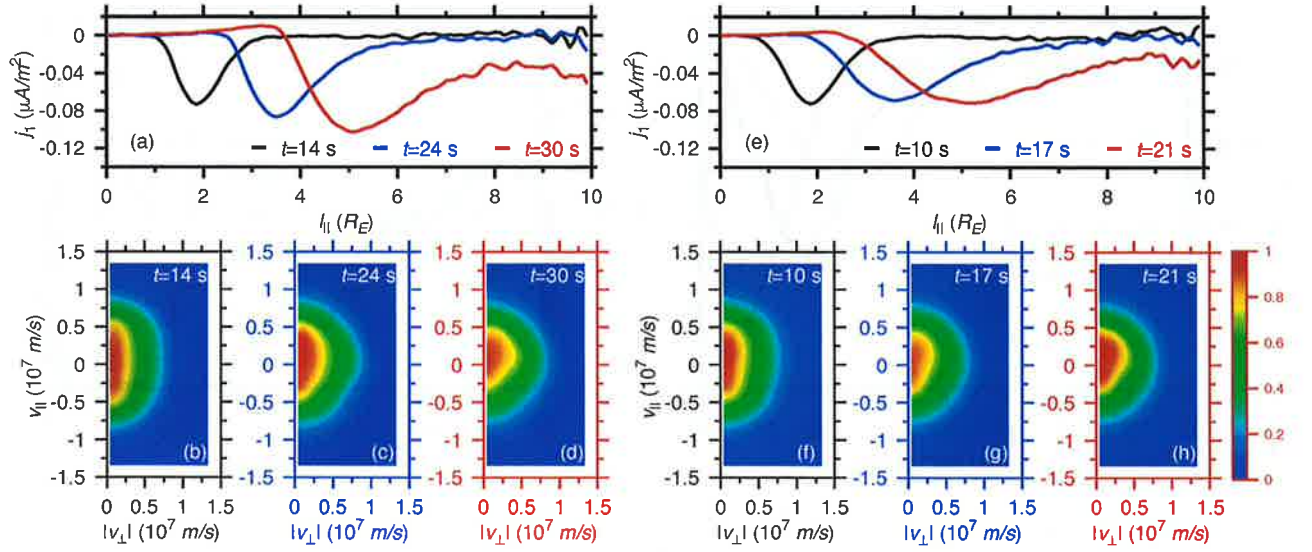
Figure 11. (a) Parallel current density along the $L = 9.7$ field line at indicated times for $T_i = 0$ case. (b) Normalized electron velocity distribution function (f_e) at $l_{||} = 2$ R_E and $t = 14$ s (black case in panel a). (c) f_e at $l_{||} = 3.5$ R_E and $t = 24$ s (blue case in panel a). (d) f_e at $l_{||} = 5$ R_E and $t = 30$ s (red case in panel a). (e) Parallel current density along field line at indicated times for $T_i = 1$ keV case. (f) f_e at $l_{||} = 2$ R_E and $t = 17$ s (black case in panel e). (g) f_e at $l_{||} = 3.5$ R_E and $t = 17$ s (blue case in panel e). (h) f_e at $l_{||} = 5$ R_E and $t = 17$ s (red case in panel e).
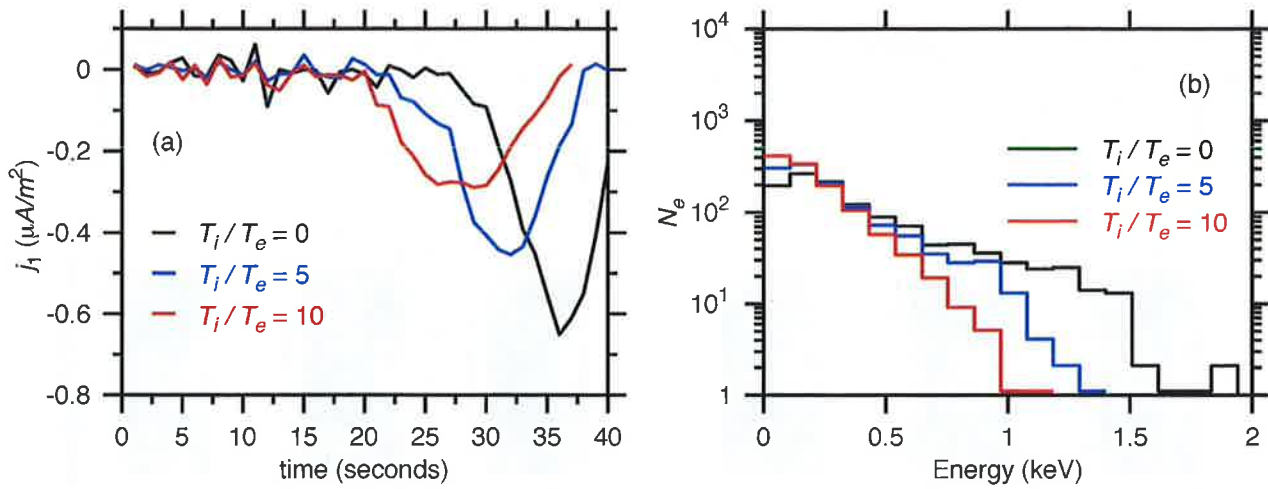
Figure 12.   a) Parallel current at the northern low altitude boundary of $L = 9.7$ field line as a function of time for three ratios of the ion to electron temperature. b) Histograms of electron kinetic energy at the peak of the parallel current in each case as indicated in Figure 12a ($t = 36$ s for $T_i/T_e = 0$, $t = 32$ s for $T_i/T_e = 5$ and $t = 30$ s for $T_i/T_e = 10$). Histograms were constructed by binning simulation electrons in 20 bins of constant energy width between 0 and 2.2 keV.

Princeton Plasma Physics Laboratory
Office of Reports and Publications

Managed by
Princeton University

under contract with the
U.S. Department of Energy
(DE-AC02-09CH11466)